D-Wave
The Quantum Computing Company™

Probing Mid-Band and Broad-Band Noise in Lower-Noise D-Wave 2000Q Fabrication Stacks

WHITEPAPER

Summary

D-Wave has been continually developing its fabrication stack in order to reduce sources of noise. Here, we present the noise assessment results for two prototype lower-noise D-Wave 2000Q fabrication stacks, recently developed as part of the low-noise quantum annealing processor development project. Using single-qubit and multi-qubit tunneling rates measurements, we compare the flux noise in lower-noise D-Wave 2000Q fabrication stacks to the baseline D-Wave 2000Q fabrication stack and show 4.3× reduction in mid-band noise and 3× reduction in broad-band noise levels. The reduced-noise levels in the newly-developed processor result in 7.4× enhancement in tunneling rates.

1 Overview

One of the main sources of decoherence in the D-Wave quantum annealing processor is flux noise, which shows up as a fluctuating bias in the double-well potential of rf-SQUID flux qubits and reduces the rate of multi-qubit tunneling processes. Following our previous noise assessment work [1–3], we have investigated the effect of the mid-band and broad-band flux noise on macroscopic resonant tunneling (MRT) of flux between the two wells of the qubit 's double-well potential by measuring the tunneling rates of single- and multi-qubit systems at different points in the annealing schedule. Quantitative modeling of tunneling rate versus flux bias traces allows us to characterize the flux noise spectral density. We performed these measurements for two circuits fabricated in the lower-noise D-Wave 2000Q fabrication stack and compared them to the baseline D-Wave 2000Q fabrication stack. We observed up to a 3× reduction in the broad-band and 4.3× reduction in the mid-band flux noise of the new processors. The mid-band and broad-band noise reductions result in 7.4× enhancement in tunneling rates.

The Effect of Noise on Tunneling Rate: The effect of flux noise on MRT profile has been discussed extensively in the previous theoretical and experimental studies [1–7]. We assume that the spectral density of flux noise $S(\omega)$ can be written as the sum of a low- and a high- frequency component: $S(\omega) = S_L(\omega) + S_H(\omega)$. As a result, the tunneling rate, Γ_{mn} between two states ($|m\rangle$ and $|n\rangle$) of our rf SQUID can be described as a convolution of two $G^L(\omega)$ and $G^H(\omega)$ functions, representing the contribution of low- and high-frequency noise [7]:

$$\Gamma_{mn}(\omega_{mn}) = \int \frac{d\omega}{2\pi} \Delta_{mn}^2 G_{mn}^L(\omega_{mn} - \omega) G_{mn}^H(\omega). \quad (1)$$

Here, Δ_{mn} is the tunneling energy and $\hbar\omega_{mn} = E_m - E_n$ is the energy difference between the two states. The contribution of the low-frequency noise to the tunneling-rate profile $G^L(\omega)$ has a Gaussian line shape with a width proportional to $W^2 = \int \frac{d\omega}{2\pi} S_L(\omega)$ and an offset proportional to $\epsilon_L \simeq W^2/2k_BT$:

$$G_{mn}^L(\omega) = \sqrt{\frac{2\pi}{a_{mn}W^2}} \cdot \exp\left[\frac{-(\hbar\omega - a_{mn}\epsilon_L)^2}{2a_{mn}W^2}\right], \quad (2)$$

where a_{mn} is the Hamming distance between the two states [1]. The low-frequency (mid-band) noise can be probed through width or peak-shift measurements.

Assuming that the high-frequency noise is due to an ohmic environment, the contribution of this noise to the profile of tunneling rate can be approximated as a Lorentzian function of S_H:

$$G^H_{mn}(\omega) = \frac{a_{mn} S_H(\omega)/\hbar}{(\hbar\omega)^2 + \left(a_{mn} S_H(0)/2\hbar\right)^2}, \tag{3}$$

in which

$$S_H(\omega) = \frac{\hbar^2 \eta \omega}{1 - e^{-\hbar\omega/k_B T}} e^{-\frac{|\omega|}{\omega_c}}. \tag{4}$$

Here, T is temperature and η is a small dimensionless parameter that can be used to characterize the coupling strength of the broad-band noise to a single- or multi-qubit system. The other parameter, ω_c, is a high frequency cutoff, defined to simplify the integration by removing the divergence. The tunneling-rate profile near degeneracy is insensitive to the exact value of ω_c. In the limit of small η, the effect of the high-frequency noise mainly shows up as excess tunneling in the tail of the tunneling-rate profile. However, larger coupling parameters ($\eta \sim \mathcal{O}(10^{-2})$) also reduce the tunneling-rate peak.

Equation 1 can be used to model the tunneling rate between any two states of rf SQUIDs for both single- and multi-qubit cases. The Gaussian low-frequency and the Lorentzian high-frequency noise terms (Eq. 2 and Eq. 3) depend only on the Hamming distance between the two states and they can be calculated easily. However, one must calculate the appropriate value of Δ_{nm} for a given experiment based on independently calibrated device parameters and use a model that accounts for the higher energy states in the individual rf SQUIDs. A more complicated SQUID model including 6 to 8 energy states is preferred when assessing the characteristics of the tunneling energy in multi-qubit systems. However, for the purpose of this work, we were primarily interested in characterizing the noise parameters by fitting data to Eq. 1. Since Δ_{nm} is simply a prefactor in this expression, we were able to treat it as a phenomenological parameter. In this case, the tunneling energy Δ_{mn} becomes proportional to the energy difference between the two lowest energy states

[1] Hamming distance between two states is the number of spins that need to be flipped in one state to match the other state.

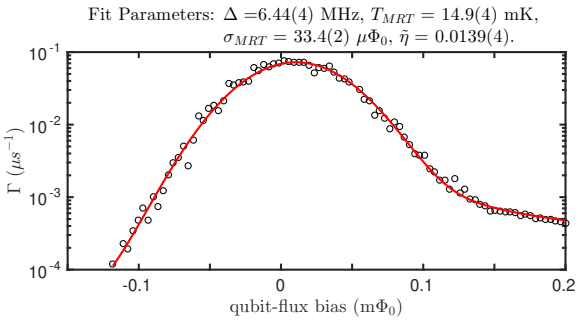

Figure 1: A sample of the single-qubit MRT measurement as a function of the external qubit flux bias (black points) and the result of an unweighted fit to a two-level single-qubit model (red line). The extracted fit parameters include the tunneling amplitude Δ/h, width W, temperature T and coupling parameter η. The cut-off frequency ω_c is fixed to 8×10^8 GHz. Uncertainties in the fit parameters are standard deviations of 10 boot-strap iterations.

at degeneracy (indicated by Δ). Assuming that the tunneling energy is small ($\Delta \ll W$), we used Eq. 1 to fit our MRT measurement results and extracted noise-dependent parameters including the width W and coupling parameter η, and other parameters including the tunneling amplitude Δ/h and temperature T. A sample of one-qubit MRT measurements and the fit results are shown in Fig. 1.

We performed a series of single- and multi-qubit MRT measurements [1, 2] on devices within D-Wave 2000Q processors that were manufactured using both the current baseline fabrication stack and two lower noise fabrication stacks. Using the single-qubit model of Eq. 1 as the fit function, we compared the extracted values for the width of the tunneling-rate profile W (induced by the mid-band noise) and coupling parameter η (induced by the broad-band noise) between the three processors. For simplicity, in our figures we will refer to these processors based on the labels shown in Table 1.

Fabrication stack	Description
FAB1	baseline 2000Q stack
FAB2-INT	interim lower-noise stack
FAB2	lower-noise stack

Table 1: Labels and description for the three fabrication stacks studied.

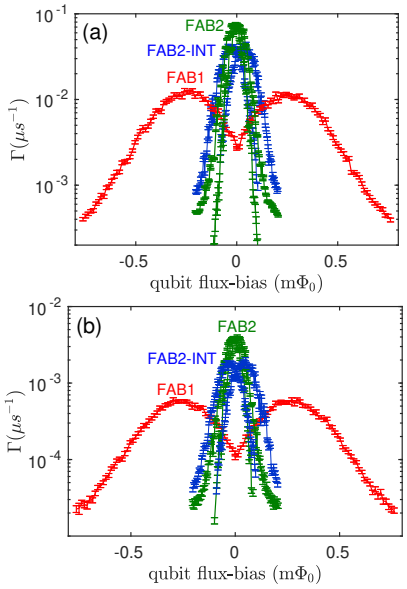

Figure 2: Single qubit MRT measurement results for the FAB1 processor (labeled in red) compared to the FAB2-INT processor (labeled in blue) and FAB2 processor (labeled in green) for similar tunneling amplitudes (obtained from fit) within the range of (a) $\Delta/h = 6.5$ to 7.0 MHz and (b) $\Delta/h = 1.5$ to 1.6 MHz. Two lobes represent the two possible initial states of the qubit ($\Gamma_{0\to1}$ and $\Gamma_{1\to0}$).

2 Mid-Band Noise Assessment

Single-Qubit Tunneling Rate Measurements: We began by performing a series of single-qubit MRT experiments for various tunneling energies Δ for all three processors. Due to bandwidth limitations and in order to avoid extremely long measurement times, we focused on evolution times between 10^0 to 10^3 μs. This placed a limit of $\Gamma \approx 0.002$ to 0.1 μs^{-1} on the dynamic range of our rate measurements and subsequently a limit of $\Delta/h \approx 0.1$ to 50 MHz on the tunneling amplitude, which satisfies the small Δ condition assumed in our analysis model. The complete set of measurements for each processor was performed for one qubit located in the middle of the processor. We verified that we were able to obtain similar results on a subset of those measurements performed on qubits located at random locations across each processor. All the measurements were performed with the dilution refrigerator mixing chamber at $T_{MXC} = 12.5$ mK.

Figure 2 shows two samples of single-qubit MRT measurements for similar tunneling amplitudes (extracted from fits) within the range of $\Delta/h = 6.5$ to 7.0 MHz (Fig. 2 (a)) and Δ/h =1.5 to 1.6 MHz (Fig. 2 (b)). The increased tunneling rate, smaller width, and smaller peak shift apparent in the single qubit MRT profiles of the new processors (blue and green curves) indicate a lower level of mid-band flux noise in these processors. To get a quantitative estimate of the magnitudes of the mid-band flux noise and broad-band ohmic noise, we fit the measurement results to a single-qubit model of Eq. 1 and extracted the noise-induced width broadening W and the coupling parameter η.

Figure 3 (a) compares the extracted widths of single qubit MRT profiles between the three processors for a number of tunneling amplitudes within the range of $\Delta/h = 0.5$ to 20 MHz. The extracted widths W for each processor remain unchanged within the Δ range of our measurements. The average width of single-qubit MRT profile of each processor is shown in Table 2. The uncertainties denote the one-sigma spread in the values. The FAB2 processor has the lowest average width, followed by the FAB2-INT processor which are, respectively, 4.3× and 3.1× smaller than the average width for the FAB1 processor.

Fabrication stack	Width [$\mu\phi_0$]
FAB1	145 ± 2
FAB2-INT	46.8 ± 0.9
FAB2	33.0 ± 0.6

Table 2: Mid-band noise induced widths extracted form fitting single-qubit MRT measurements to Eq. 1.

Multi-Qubit Tunneling Rate Measurements: We also measured MRT of two-, three- and four-qubit clusters. The qubits are coupled in a linear configuration with an effective mutual inductance of $M_{eff} = -4$ pH between pairs of qubits. To analyze the multi-qubit MRT data, we still used the two-level single-qubit model of the tunneling-rate function (Eq. 1) as the fit function.

Figure 3 (b) compares the average values of the width W between the three processors as a function of the number of qubits N. The ratio of widths between different processors is approximately constant as the number of qubits grows and the results scale as $\sqrt{N}$ for each. This observation provides evidence that the noise amplitude within a cluster of strongly coupled qubits is the incoherent sum of the noise in the individual qubits,

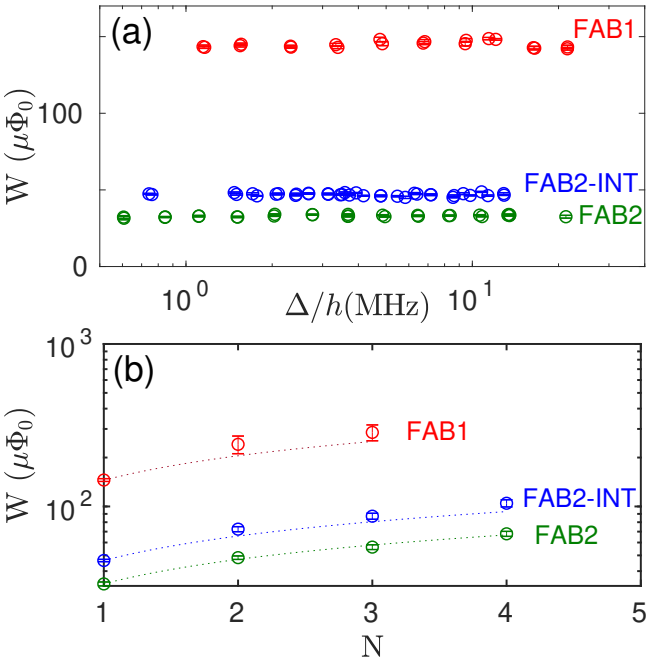

Figure 3: Mid-band noise assessment: (a) comparison of the mid-band noise-induced widths W, obtained from fits to Eq. 1, for a series of single-qubit MRT measurements within the tunneling amplitude range of $\Delta/h = 0.5$ to 20 MHz. Error bars are smaller than data markers. Compared to the average width of $W = 145(2)\ \mu\phi_0$ for the FAB1 processor (red), the average width of the MRT profile for the FAB2 (green) is 4.3× smaller and for the FAB2-INT (blue) is 3.1× smaller. (b) The average width of the MRT profile (extracted from fit to a series of multi-qubit MRT measurements at similar tunneling amplitude ranges as before) as a function of the number of qubits N for FAB1 (red), FAB2-INT (blue) and FAB2 (green) processor. The dotted lines indicate $\sqrt{N}W_{1q}$.

as concluded in [2].

3 Broad-Band Noise Assessment

Single-Qubit Tunneling Rate Measurements: To assess the broad-band noise, we compared the extracted values of the coupling parameter η between the three processors (see Fig. 4). The average value of the single qubit broad-band coupling parameter η for each processor is shown in Table 3. The uncertainties denote the one-sigma spread in the values. Similar to the

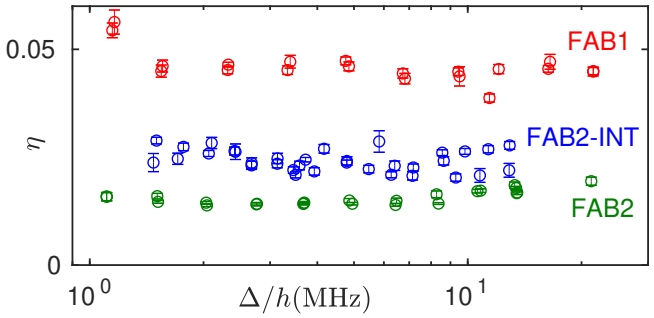

Figure 4: Broad-band noise assessment: comparison of the high-frequency noise coupling parameter η, obtained from fit, for a series of single-qubit MRT measurements within the tunneling amplitude range of $\Delta/h = 0.1$ to 20 MHz. The broad-band noise coupling parameters of the FAB2 processor (green) and the FAB2-INT processor (blue) are, respectively, 3× and 2× smaller than the average value of $\eta = 0.047(4)$ obtained for the FAB1 processor (red).

mid-band noise assessment results, the FAB2 processor has the lowest average broad-band noise coupling, followed by the FAB2-INT processor, which are, respectively, 3× and 2× smaller than the FAB1 processor.

Fabrication stack	Coupling-parameter η
FAB1	0.047 ± 0.004
FAB2-INT	0.024 ± 0.003
FAB2	0.016 ± 0.002

Table 3: Broad-band coupling parameter extracted form fitting single-qubit MRT measurements to Eq. 1.

4 Tunneling-Rate Assessment

The single-qubit model of Eq. 1 predicts the effect of the mid-band and broad-band noise on the maximum tunneling rate as [3]:

$$\Gamma_{max} \propto \frac{(\frac{\pi k_B T}{\hbar\omega_c})^{\eta} \cdot \Delta^2}{W}. \quad (5)$$

Due to the Gaussian characteristic of the mid-band noise, Γ_{max} is proportional to the inverse of the mid-band noise induced width W. In the limit of small coupling parameters ($\eta < \mathcal{O}(10^{-3})$), the prefactor $(\frac{\pi k_B T}{\hbar\omega_c})^{\eta}$ approaches 1 and only the mid-band noise contributes to the tunneling-rate peak. However, for the obtained

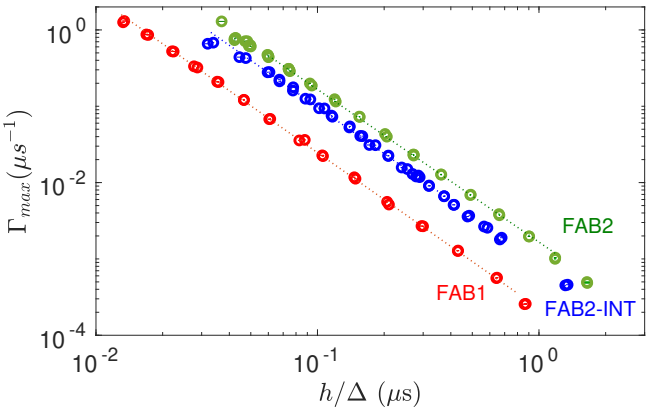

Figure 5: Comparison of the single-qubit maximum tunneling rate Γ_{max} between FAB1 (red), FAB2-INT (blue) and FAB2 (green) processor vs. the inverse of tunneling amplitude Δ/h. The dotted lines represent the linear fit to one-qubit measurements.

range of the broad-band coupling parameters in our processors, both mid-band and broad-band noise are expected to contribute.

Figure 5 compares the maximum tunneling rate Γ_{max} of a single qubit between three processors as a function of the inverse of tunneling amplitude h/Δ (obtained from a fit). To estimate the enhancement in the tunneling performance of the newly developed processors, we compared the offset values of linear fits to $\log\Gamma_{max}$ vs. $\log(h/\Delta)$. The slope and offset values of the fit to single-qubit MRT measurements of each processor are shown in Table 4.

Fabrication stack	Slope (A)	Offset (B)
FAB1	-2.04 ± 0.14	-8.4 ± 0.4
FAB2-INT	-2.03 ± 0.16	-7.0 ± 0.3
FAB2	-2.00 ± 0.13	-6.4 ± 0.3

Table 4: Slope (A) and offset (B) of a linear fit $\log\Gamma_{max} = A\log(h/\Delta) + B$ to one-qubit MRT measurement results. The maximum tunneling-rate ratio between processors at any given tunneling-energy Δ was obtained by comparing the exponential of offsets (e^B).

The maximum tunneling rate at a given tunneling energy for a single qubit in the FAB2 processor is 7.4× and in the FAB2-INT processor is 4× larger than the FAB1 processor. The enhanced tunneling rates of the newly developed processors are achieved as a result of a reduction in both mid-band and broad-band noise as predicted.

5 Conclusion

In conclusion, we used MRT experimental measurements to compare the mid-band and broad-band noise for two of our newly-developed processors in the lower-noise D-Wave 2000Q fabrication stack to a current one in the baseline D-Wave 2000Q fabrication stack. We showed up to a 3× reduction in broad-band noise and 4.3× reduction in mid-band noise, which translate to 7.4× enhancement in tunneling rates. We also showed that in all three tested processors, the coupling of the mid-band noise to each qubit is uncorrelated to the other qubits in that processor.

References

1 R. Harris, M. W. Johnson, S. Han, A. J. Berkley, J. Johansson, et al., "Probing noise in flux qubits via macroscopic resonant tunneling," Phys. Rev. Lett. **101**, 117003 (2008).

2 T. Lanting, R. Harris, J. Johansson, M. H. S. Amin, A. J. Berkley, et al., "Cotunneling in pairs of coupled flux qubits," Phys. Rev. B **82**, 060512 (2010).

3 T. Lanting, M. H. S. Amin, M. W. Johnson, F. Altomare, A. J. Berkley, et al., "Probing high-frequency noise with macroscopic resonant tunneling," Phys. Rev. B **83**, 180502 (2011).

4 M. H. S. Amin and D. V. Averin, "Macroscopic resonant tunneling in the presence of low frequency noise," Phys. Rev. Lett. **100**, 197001 (2008).

5 S. Boixo, V. N. Smelyanskiy, S. V. Isakov, M. Dykman, V. S. Denchev, M. H. Amin, A. Y. Smirnov, M. Mohseni, and H. Neven, "Computational multiqubit tunnelling in programmable quantum annealers," Nature Communications **7** (2016).

6 C. M. Quintana, Y. Chen, D. Sank, A. G. Petukhov, T. C. White, et al., "Observation of classical-quantum crossover of $1/f$ flux noise and its paramagnetic temperature dependence," Phys. Rev. Lett. **118**, 057702 (2017).

7 A. Y. Smirnov and M. H. Amin, "Theory of open quantum dynamics with hybrid noise," New Journal of Physics **20**, 103037 (2018).